

## Article

# Multiple Linear Regression Models with Limited Data for the Prediction of Reference Evapotranspiration of the Peloponnese, Greece

Stavroula Dimitriadou and Konstantinos G. Nikolakopoulos \* 

Department of Geology, University of Patras, 26504 Patras, Greece; sdhm@upatras.gr

\* Correspondence: knikolakop@upatras.gr; Tel.: +30-2610997592

**Abstract:** The aim of this study was to investigate the utility of multiple linear regression (MLR) for the estimation of reference evapotranspiration (ET<sub>o</sub>) of the Peloponnese, Greece, for two representative months of winter and summer during 2016–2019. Another objective was to test the number of inputs needed for satisfactorily accurate estimates via MLR. Datasets from sixty-two meteorological stations were exploited. The available independent variables were sunshine hours (N), mean temperature (T<sub>mean</sub>), solar radiation (R<sub>s</sub>), net radiation (R<sub>n</sub>), wind speed (u<sub>2</sub>), vapour pressure deficit (es – ea), and altitude (Z). Sixteen MLR models were tested and compared to the corresponding ET<sub>o</sub> estimates computed by FAO-56 Penman–Monteith (FAO PM) in a previous study, via statistical indices of error and agreement. The MLR5 model with five input variables outperformed the other models (RMSE = 0.28 mm d<sup>-1</sup>, adj. R<sup>2</sup> = 98.1%). Half of the tested models (two to six inputs) exhibited very satisfactory predictions. Models of one input (e.g., N, R<sub>n</sub>) were also promising. However, the MLR with u<sub>2</sub> as the sole input variable presented the worst performance, probably because its relationship with ET<sub>o</sub> cannot be linearly described. The results indicate that MLR has the potential to produce very good predictive models of ET<sub>o</sub> for the Peloponnese, based on the literature standards.



**Citation:** Dimitriadou, S.; Nikolakopoulos, K.G. Multiple Linear Regression Models with Limited Data for the Prediction of Reference Evapotranspiration of the Peloponnese, Greece. *Hydrology* **2022**, *9*, 124. <https://doi.org/10.3390/hydrology9070124>

Academic Editor: Marco Delle Rose

Received: 31 May 2022

Accepted: 11 July 2022

Published: 12 July 2022

**Publisher's Note:** MDPI stays neutral with regard to jurisdictional claims in published maps and institutional affiliations.



**Copyright:** © 2022 by the authors. Licensee MDPI, Basel, Switzerland. This article is an open access article distributed under the terms and conditions of the Creative Commons Attribution (CC BY) license (<https://creativecommons.org/licenses/by/4.0/>).

**Keywords:** multiple linear regression; linear regression; FAO Penman–Monteith; reference evapotranspiration; Peloponnese; Greece

## 1. Introduction

Reference evapotranspiration (ET<sub>o</sub>) as a climate parameter plays a pivotal role in climate crisis research and in water resources management. There are complex interactions between evapotranspiration and key environmental components, such as groundwater and streamflow, as well as with anthropogenic and climatic impacts, such as wildfires, air pollution, land use/land cover (LULC) change, crop intensification, and construction [1–4]. Moreover, ET<sub>o</sub> is directly related to the productive sector of agriculture, since crop water needs are usually estimated as a function of ET<sub>o</sub> with a crop-specific coefficient [5]. Irrigation system design and precision irrigation techniques demand accurate determination of ET<sub>o</sub> [6,7]. Since the management of finite resources such as water is challenging, the exploitation of accurate predictive tools of ET<sub>o</sub>, which are still easy to apply, is of major importance in an interdisciplinary context [8–10]. Another important contribution of ET<sub>o</sub> is its use in computing actual evapotranspiration, which is difficult to acquire [11,12].

The measurement of the ET<sub>o</sub> is demanding. Therefore, several methods for estimating ET<sub>o</sub> have been developed, ranging from simple empirical or physically based models [13,14] to complex algorithms and techniques, such as fuzzy logic and machine learning (ML) [15–21]. These methods employ data from meteorological stations, or retrieved data via remote sensors [22–32]. The FAO-56 Penman–Monteith (FAO PM) equation (Equation (1)) is the most established method used to compute ET<sub>o</sub> worldwide. How-

ever, it requires a large number of meteorological variables, which are not always easy to retrieve [33,34].

$$ET_o = \frac{0.408 \cdot \Delta (R_n - G) + \gamma \frac{900}{T+273} \cdot u_2 (e_s - e_a)}{\Delta + \gamma (1 + 0.34 \cdot u_2)} \quad (1)$$

where  $R_n$  is the net radiation ( $\text{MJ m}^{-2} \text{d}^{-1}$ ),  $G$  is the soil heat flux ( $\text{MJ m}^{-2} \text{d}^{-1}$ ),  $T$  is the air temperature ( $^{\circ}\text{C}$ ),  $e_s - e_a$  is the vapour pressure deficit (kPa),  $\Delta$  is the slope of the vapour pressure curve ( $\text{kPa } ^{\circ}\text{C}^{-1}$ ),  $u_2$  is the wind speed at 2 m distance from the surface ( $\text{m s}^{-1}$ ), and  $\gamma$  is the psychrometric constant ( $\text{kPa } ^{\circ}\text{C}^{-1}$ ) [33].

On the other hand, there is a handful of empirical methods in the literature utilising limited climatic parameters (e.g., the Hargreaves–Samani equation [35]). However, FAO PM usually outperforms them in terms of accuracy and consistency, especially over different seasons of the year [36]. As a general rule, the level of prediction accuracy generally improves with the increase in input parameters [37]. The cost of the necessary sensors, the equipment, and the maintenance of meteorological stations, along with the difficult environmental conditions at several regions, result in data unavailability or at least scarcity, especially for the developing countries. Therefore, an effort to reduce the quantity of data required for predictive models is highly recommended, provided that satisfactory accuracy is secured [38]. Air temperature (minimum, maximum, and mean values) is the most basic parameter. In a parsimonious prospect, parameters that are suitable explanatory variables for  $ET_o$  modelling can be easily measured (i.e., air temperature), or can be either measured or computed (i.e., wind speed, solar and net radiation, sunshine hours, vapour pressure deficit). The computation of any missing data can be carried out using air temperature, Julian day, and latitude, according to FAO guidelines [33,39,40].

Among the highly complex methods that have been tested lately, multiple linear regression (MLR) has been suggested by a number of recent studies as an adequate method for estimating climatic parameters such as air temperature, growing degree days, and solar radiation [41–44]. Remotely sensed data, especially MODIS and Landsat products, have gained ground in MLR modelling lately, as inputs for the estimation of climatic parameters, such as land surface temperature and surface urban heat island [45–47]. The added value of MLR is that it is a simple, comprehensible method, producing easily interpretable results, while requiring short real-time control and low computational effort [48]. The challenge lies in the ability of MLR to produce sufficiently accurate predictions of  $ET_o$  over an area with inhomogeneous LULC types and relief, and which presents distinguished differences in meteorological parameters over short distances (<http://climatlas.hnms.gr/sdi/?lang=EN> (accessed on 3 May 2022)) [36].

The recent relevant literature is rather limited compared to more complex methods such as artificial neural networks (ANNs). Perugu et al. developed MLR models to estimate  $ET_o$  for Andhra Pradesh, India, based on temperature, sunshine hours, wind speed, and relative humidity as independent variables [49]. They put forward these models for regions with similar climatic conditions. The regression models developed earlier by Mallikarjuna et al. for the same area, utilizing the same explanatory variables, also showed a satisfactory performance in  $ET_o$  estimation at daily scale (i.e.,  $R^2$  between 89.1–97% and RMSE between 0.26–0.49  $\text{mm d}^{-1}$ ) [50]. Khoshravesh et al. applied non-linear and Bayesian regression models for three arid regions in Iran, and the best results they yielded were  $R^2 > 95\%$  and a RMSE of about 4.00  $\text{mm d}^{-1}$  [51]. Tabari et al. evaluated the performances of neuro-fuzzy models, multiple linear regression, and multiple non-linear regression models, along with temperature-based and radiation-based models for a semi-arid region in Iran [52]. The model with mean temperature, solar radiation, wind speed, and relative humidity as inputs displayed the best performance (RMSE = 0.552  $\text{mm d}^{-1}$ ,  $R^2 = 96\%$ , and MAE = 0.442  $\text{mm d}^{-1}$ ). The model with only mean air temperature as an input produced the poorest estimates. The non-linear regression improved RMSE,  $R^2$ , and MAE to 0.452  $\text{mm d}^{-1}$ , 97.6%, and 0.331  $\text{mm d}^{-1}$ , respectively. These values were considered acceptable for MLR predictions of  $ET_o$  in a semi-arid region [52]. Shirsath and Singh found that all MLR models outperformed the climate-based Penman, Priestley–

Taylor, and Stephens and Stewart models in predicting daily pan evaporation, although the best values of the evaluating measures were  $R^2 = 61\%$  and  $RMSE = 1.597 \text{ mm d}^{-1}$  [53]. These MLR models were slightly less accurate than the corresponding comparative ANN models. Sanford et al. developed MLR equation with climate parameters (minimum and maximum temperature and precipitation) at an annual scale (1971–2000) for Virginia watersheds with  $R^2 = 84.4\%$  [54]. The MLR equation was modified in a following study using these parameters to estimate the ET/P ratio, yielding an  $R^2$  value of 86.74% and an  $RMSE = 0.067 \text{ mm d}^{-1}$  for the best-fit parameters for the conterminous US [55]. The obtained values were considered satisfactory for explaining most of the variation in long-term average ETo across the conterminous US [55]. Although most recent articles do not employ MLR to the assessed models, Niaghi et al. applied MLR to datasets of six stations at Red River Valley [56]. They grouped the input combinations into air temperature-based (Tmax, Tmin), mass transfer-based (Tmax, Tmin, wind speed), and radiation-based (solar radiation, Tmax, Tmin) measurements. The best performance for MLR models was for the latter inputs ( $RMSE = 0.68 \text{ mm d}^{-1}$ ,  $MAE = 0.51 \text{ mm d}^{-1}$ , and  $R^2 = 88\%$ ). The MLR models were not sensitive to differences between local and spatial applications compared to the heuristic models, due to their inability to depict complex relationships [56]. Ohana-Levi et al. found that the six linear regression models had much higher RMSE values than the corresponding non-linear multivariate adaptive regression spline (MARS) models [57]. The correlation coefficients during training and testing were 0.84 and 0.85, respectively, for the linear models [57]. In MLR models where leaf area index (LAI) was added as an explanatory variable, the testing RMSE profoundly improved when using the Kc approach (the RMSE of  $1.05 \text{ mm d}^{-1}$  without LAI reduced to  $0.81 \text{ mm d}^{-1}$ ) [57]. Sharafi and Ghaleni compared the performance of six MLR models to empirical methods. They found that all the MLR models outperformed the latter [58]. The obtained RMSE values, ranging between  $0.36 \text{ mm d}^{-1}$  and  $0.50 \text{ mm d}^{-1}$ , were considered excellent, so that MLR was recommended for all climate types of Iran, from arid desert to humid [58]. An MLR model of precipitation, temperature, soil moisture, and NDVI as explanatory variables was applied to four basins in India [59]. The ETo variance was explained by 82–91% (adj.  $R^2$ ) via the utilised MLR model [59]. The MLR stepwise modelling applied at the Inner Mongolia Autonomous Region (1971–2016) demonstrated that the ETo values in different regions were affected by different climatic parameters [60]. It is noteworthy that ETo was found insensitive to mean air temperature for the whole area [60]. For the Megecha catchment in Ethiopia, sunshine hours, wind speed, maximum temperature, and relative humidity were proven to be the best explanatory variables of ETo in MLR modelling [61].

This study examines sixteen MLR models utilizing data from sixty-two meteorological stations in the Peloponnese, a southwestern region of Greece (Table A1). The Peloponnese constitutes a challenging testbed for ETo research, since it presents considerable inhomogeneities regarding relief, LULC, altitude, etc. The empirical methods of a previous study exhibited inconsistency in terms of accuracy, with larger errors found for August (summertime) [36]. As described, MLR is not very popular in recent literature of ETo. This is probably because of the complex nature of ETo. However, the added value of MLR is the simplicity and the comprehensibility of the method and the equations produced. Furthermore, it is of importance to examine whether limited data (even one sole input variable) can predict ETo satisfactorily. The latter would be useful for cases with sparse data availability. Therefore, MLR for ETo estimation needs to be further investigated since it would be a promising alternative, being easily applicable and interpretable for interdisciplinary research and management purposes.

## 2. Materials and Methods

### 2.1. The Study Area

The Peloponnese peninsula of southwest Greece occupies about 1/6th of the Greek territory ( $21,439 \text{ km}^2$ ), with a population of 1,086,935 (census 2011; <https://www.statistics.gr/el/statistics/-/publication/SAM03/2011> (accessed on 19 April 2022)). The area is

mostly hilly and mountainous. Moving from coastline to the mainland, the altitude reaches 2407 m. Its lithology, along with tectonic activity and climatic conditions, has resulted in the formation of relief. The hydrographic network is well-developed, though with few large rivers [62]. The most populated urban area is located at the northernmost edge, while the broadest plain covers the northwest. Except from urban areas, which are sparsely distributed primarily along the coastline, the main LULC types are forests, transitional vegetation, and various crop plots (Figure 1) [63]. According to the Köppen–Geiger classification, Peloponnese’s climate is Mediterranean, warm, with dry summers and mild winters (classified as Csa) [64]. The annual average (1971–2000) precipitation, air temperature, and sunshine hours range between 400 to over 2000 mm, 8–20 °C, and 1900–3100 h, respectively (<http://climatlas.hnms.gr/sdi/?lang=EN> (accessed on 3 May 2022)).

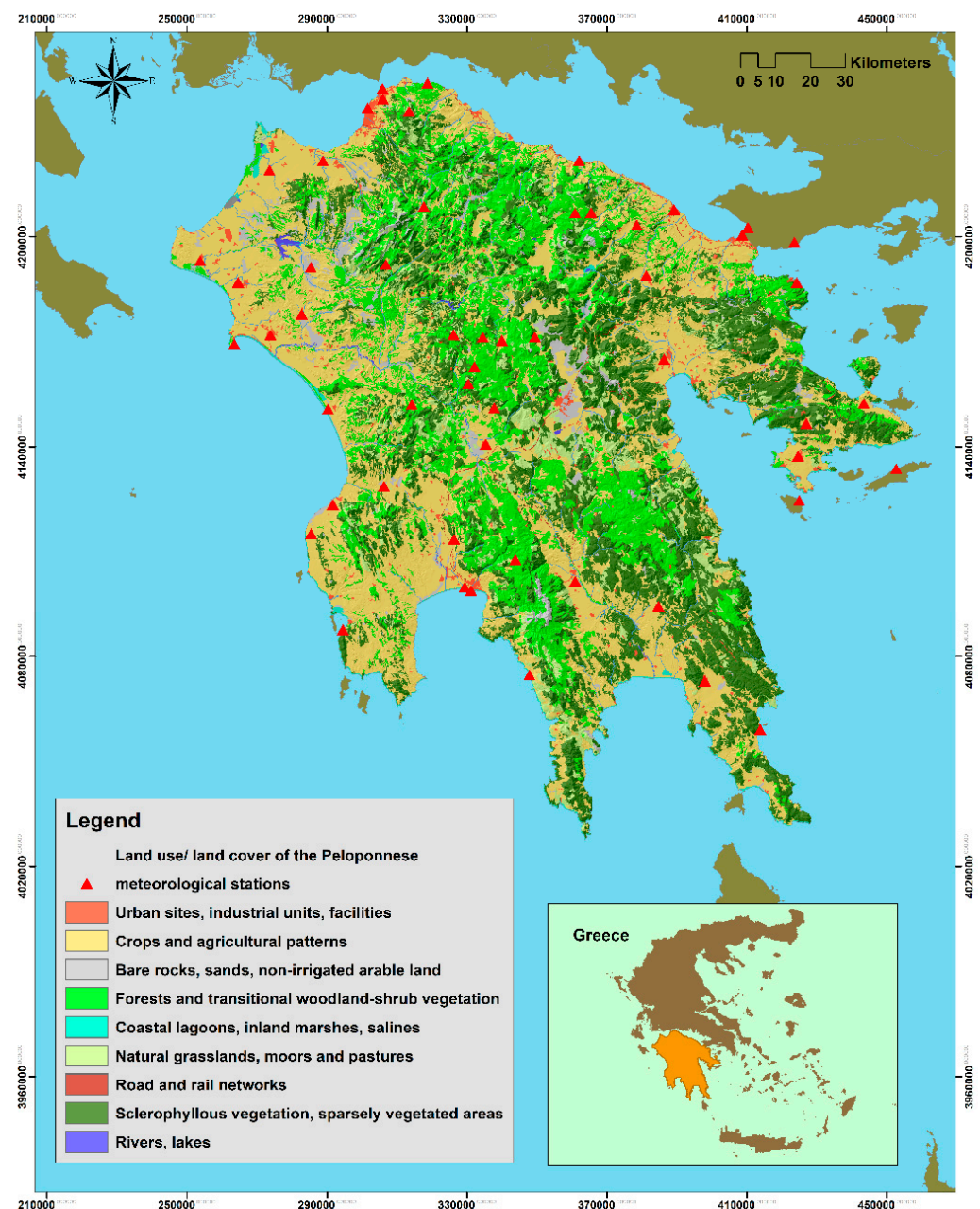


**Figure 1.** LULC map of the Peloponnese (Adapted with permission from ref. [63] 2018, © European Union).

## 2.2. Methods

Ground-based datasets of daily scale from sixty-two meteorological stations running under the National Observatory of Athens, for the months August and December of 2016–2019 were utilised (Figure 1, Table A1). The selected period exhibits interest in the context of climate crisis, since the two warmest years (2016 and 2019) since the pre-industrial era are included (<https://climate.copernicus.eu/copernicus-2019-was-second-warmest-year-and-last-five-years-were-warmest-record> (accessed on 23 June 2022)). August and December were selected as representative months of summertime and wintertime respectively (<http://climatlas.hnms.gr/sdi/?lang=EN> (accessed on 3 May 2022)), in methodological consistency with our previous study [36], aiming the results to be directly comparable. In the former study, ETo was computed for the Peloponnese by FAO PM, which serves as our reference method. In this study, multiple linear stepwise regression has been applied with seven explanatory (independent) variables, namely mean air temperature ( $T_{\text{mean}}$ ), wind speed at 2 m distance from the surface ( $u_2$ ), solar radiation ( $R_s$ ), net radiation ( $R_n$ ), sunshine hours ( $N$ ), and vapour pressure deficit ( $es - ea$ ). In addition to the climate variables, altitude ( $Z$ ) was also used as an input variable, since it indirectly affects ETo [65].  $R_s$ ,  $R_n$ ,  $N$ , and  $es - ea$  were previously calculated as in Zanetti et al. [40], based on FAO guidelines for missing climate data (functions of Julian date and station latitude) [33]. Since the need to limit the required variables in ETo modelling is underlined in the recent literature [66], the possibility of only a few variables or even only the most easy-to-acquire variable,  $T_{\text{mean}}$ , to produce satisfactorily accurate predictions of ETo for the Peloponnese was investigated. MLR as a statistical technique employs several explanatory variables and one response (dependent) variable, which is ETo in the present study. The aim of MLR is to model the linear relationship between the explanatory variables and the response variable, as an extension of ordinary least squares regression, since it incorporates more than one explanatory variable. In other words, MLR aims to find the linear function that minimizes the sum of the squares of errors (SSE) between the observed and the predicted data. An advantage of this method is the easy interpretation of the coefficients, which are generated in the model with low computational effort, in comparison to more complex techniques, such as energy balance methods and artificial intelligence algorithms [13–21,24–30,37–43,67–75]. For the MLR model, the response (dependent) variable  $y$  is assumed to be a function of  $k$  independent variables  $x_i$ . The general form of the equation is computed as follows (Equation (2)):

$$y_i = b_0 + b_1x_1 + \dots + b_kx_k + e \quad (2)$$

where  $b_0$  and  $b_i$  stand for the fitting constants;  $x_i$  represents the  $i$ th observation of each of the explanatory variables,  $y_i$  stands for the  $i$ th prediction of ETo, and  $e_i$  is a random error term representing the remaining effects of variables on  $y$ , which are not covered by the model (residuals). The least squares criterion for the minimum sum of squares of error terms is usually applied to determine the fitting constants [61]. Stepwise MLR has the advantage of presenting the MLR models, beginning from the most influential parameter of the input combination (which explains the larger percentage of ETo variability, expressed by  $\text{adj. } R^2$ ) [60]. It presents the models in ascending order of  $\text{adj. } R^2$ , and it may omit several input variables in case they do not meaningfully contribute to the variability explanation. This meaningful contribution of one variable is determined via the  $\text{adj. } R^2$ , as opposed to  $R^2$ , which generally increases with the number of inputs. Therefore,  $\text{adj. } R^2$  and  $R^2$  are not directly comparable, since the latter would generally have a greater value than the former (Table 1).

**Table 1.** The statistical measures employed to evaluate the performance of the regression models.

Formulae of the Indices	
$RMSE = \sqrt{\frac{\sum_{i=1}^n (P_i - r_i)^2}{n}} \quad (2)$	$NRMSE = \frac{\sqrt{\frac{\sum_{i=1}^n (P_i - r_i)^2}{n}}}{\bar{r}} \quad (3)$
$MAE = \frac{\sum_{i=1}^n  P_i - r_i }{n} \quad (4)$	$adj.R^2 = 1 - \frac{(1-R^2)(1-n)}{n-k-1} \quad (5)$
$R^2 =$ $\left( \frac{n \sum_{i=1}^n P_i \cdot O_i - \sum_{i=1}^n P_i \cdot \sum_{i=1}^n O_i}{\sqrt{n \sum_{i=1}^n P_i^2 - (\sum_{i=1}^n P_i)^2} \cdot \sqrt{n \sum_{i=1}^n O_i^2 - (\sum_{i=1}^n O_i)^2}} \right)^2 \quad (6)$	$IoA = 1 - \frac{\sum_{i=1}^n (P_i - r_i)^2}{\sum_{i=1}^n ( P_i - \bar{r}  -  r_i - \bar{r} )^2} \quad (7)$

The predicted ETo values from the regression models were then compared against the values of FAO PM via statistical indices (Table 1). Specifically, the error levels between predicted and reference values were computed via measures such as root mean square error (RMSE, mm d<sup>-1</sup>), normalised root mean square error (NRMSE, %), mean absolute error (MAE, mm d<sup>-1</sup>), and standard error of the predicted value (SE, mm d<sup>-1</sup>) (Table 1, Equations (2)–(4)). The error values follow the magnitude of the computed ETo values, except for NRMSE, which is expressed in \*100% (Table 1, Equation (3)). Moreover, two measures that express the percentage of ETo variability explained by the independent variables of the model and the agreement between predicted and reference values were utilised, namely the adjusted coefficient of determination (adj. R<sup>2</sup>) and the index of agreement (IoA) (Table 1, Equations (5) and (7)). These measures are suitable for statistical analyses of evapotranspiration, [57,76,77]. At last, residual analysis was performed using the Durbin–Watson index (D–W), Cook’s Distance (Cook’s D), and Centred Leverage. D–W is used to detect the presence of autocorrelation in the residuals. Values around 2.0 (usually between 1.50 and 2.50) express normality, meaning negligible correlation among residuals. Lower (higher) values express positive (negative) correlation. Cook’s D values greater than 0.5 indicate potential outlier, and C. Leverage (between 0 and (k – 1)/k) is used to detect particular influential points.

In Table 1, p<sub>i</sub> stands for the *i*th value predicted by the regression model, r<sub>i</sub> stands for the *i*th reference value computed by FAO PM,  $\bar{r}$  is the mean reference value, k is the number of the independent variables, and the sample size (n) is 290.

### 3. Results

MLR models with all the potential input combinations, from one to six explanatory variables, were tested. In total, sixteen models were examined. Models with altitude or latitude as sole input variables were not applicable, whereas models with seven inputs exhibited statistically insignificant results (*p* > 0.05). The obtained results are presented in Table 2.

As portrayed in Table 2, half of the tested models (8) yielded RMSE values below 0.35 mm d<sup>-1</sup> and adj. R<sup>2</sup> values greater than 97.1% (Table 2). Among these models, MLR4, MLR5, and MLR6 obtained an RMSE below 0.29 mm d<sup>-1</sup>, and an adj. R<sup>2</sup> between 98% and 98.1%. The results for the majority of the models are statistically significant at the 99% confidence level. Only four models (MLR10, MLR11, MLR13, MLR15) yielded one coefficient that was statistically significant at the 95% confidence level. Regarding the statistical analysis of the residuals performed for each model, C. Leverage and Cook’s D were generally low, as were the SEs of the predicted values (Table 2).

MLR5 and MLR6 with five and six independent variables, respectively, have the (same) highest adj. R<sup>2</sup> (98.1%). As anticipated, MLR6, which includes one extra independent variable, obtained slightly better RMSE/NRMSE values than MLR5 (0.276 mm d<sup>-1</sup>/8.2% vs. 0.280 mm d<sup>-1</sup>/8.3%). The two models have the same MAE (0.206 mm d<sup>-1</sup>) and IoA (99.5%). The model with the highest adj. R<sup>2</sup> (98.1%) with the fewer inputs is therefore MLR5, which is a function of N, Tmean, u<sub>2</sub>, es – ea, and Rn. The former means that these five variables play a significant role in the prediction of ETo for the Peloponnese. The addition of altitude (Z) as

an extra independent variable of the model (MLR6) deteriorated the aforementioned indices, without increasing the explanation of the variance (adj.  $R^2 = 98.1\%$ ). The contribution of Z to the adj.  $R^2$  change was about 0.03%. The equation produced by the model with the best performance (MLR5) is presented in Table 3.

**Table 2.** The 16 regression models and the corresponding indices of performance.

Models	Independent Variables	Sig.	Adj. $R^2$	D–W	Cook's D	C. Leverage	SE	RMSE	NRMS	MAE	IoA
MLR1	N	<0.001	0.960	1.742	0.003 ± 0.006	0.003 ± 0.0001	0.034 ± 0.0003	0.409	0.121	0.320	0.990
MLR2	N, Tmean	<0.001	0.971	1.732	0.004 ± 0.010	0.007 ± 0.004	0.035 ± 0.006	0.343	0.102	0.248	0.993
MLR3	N, Tmean, $u_2$	<0.001	0.975	1.675	0.004 ± 0.011	0.010 ± 0.015	0.036 ± 0.011	0.321	0.095	0.238	0.994
MLR4	N, Tmean, $u_2$ , es – ea	<0.001	0.980	1.784	0.005 ± 0.014	0.014 ± 0.016	0.036 ± 0.011	0.286	0.085	0.214	0.995
MLR5	N, Tmean, $u_2$ , es – ea, Rn	<0.001	0.981	1.738	0.004 ± 0.014	0.017 ± 0.018	0.039 ± 0.011	0.280	0.083	0.206	0.995
MLR6	N, Tmean, $u_2$ , es – ea, Rn, Z	<0.001	0.981	1.746	0.005 ± 0.014	0.021 ± 0.019	0.044 ± 0.012	0.276	0.082	0.206	0.995
MLR7	Rn	<0.001	0.955	2.093	0.003 ± 0.006	0.003 ± 0.001	0.036 ± 0.003	0.429	0.127	0.323	0.989
MLR8	Rn, $u_2$	<0.001	0.969	1.949	0.004 ± 0.007	0.007 ± 0.011	0.035 ± 0.010	0.357	0.106	0.280	0.992
MLR9	Rn, $u_2$ , Tmean	<0.001	0.975	1.952	0.005 ± 0.019	0.010 ± 0.013	0.036 ± 0.011	0.321	0.095	0.251	0.994
MLR10	Rn, $u_2$ , Tmean, Z	<0.05	0.975	1.904	0.005 ± 0.015	0.014 ± 0.014	0.041 ± 0.011	0.318	0.094	0.249	0.994
MLR11	Rn, $u_2$ , Tmean, Z, Rs	<0.05	0.976	1.922	0.005 ± 0.016	0.017 ± 0.016	0.042 ± 0.012	0.313	0.093	0.245	0.994
MLR12	Tmean	<0.001	0.918	1.857	0.003 ± 0.004	0.003 ± 0.002	0.048 ± 0.008	0.582	0.172	0.461	0.978
MLR13	Tmean, $u_2$	<0.05	0.920	1.842	0.007 ± 0.046	0.007 ± 0.012	0.056 ± 0.018	0.574	0.170	0.467	0.979
MLR14	Rs	<0.001	0.918	2.098	0.003 ± 0.006	0.003 ± 0.002	0.048 ± 0.006	0.582	0.172	0.442	0.978
MLR15	$u_2$	<0.05	0.030	0.122	0.003 ± 0.003	0.003 ± 0.012	0.154 ± 0.064	2.001	0.592	1.953	0.120
MLR16	es – ea	<0.001	0.817	1.884	0.003 ± 0.007	0.003 ± 0.003	0.071 ± 0.014	0.868	0.257	0.637	0.947

Note: Sig., significance ( $p$ -value); D–W, Durbin–Watson; Cook's D, Cook's Distance; SE, standard error of the predicted value; and C. Leverage, Centred Leverage. All values are presented as mean ± SD.

**Table 3.** Formulae of the MLR model with the best performance (MLR5) and the two most accurate models with one input (MLR1, MLR7).

Model	Multiple Linear Regression Equation	Adj. $R^2$
MLR5	$ETo = -9.166 + 1.066 * N + 1.284 * (es - ea) + 0.064 * u_2 + 0.031 * Tmean$ (2)	0.981 *
MLR1	$ETo = -8.188 + 1.011 * N$ (3)	0.960 *
MLR7	$ETo = 0.494 + 0.033 * Rn$ (4)	0.955 *

Note: \* Sig. < 0.001.

Models MLR1, MLR7, MLR14, MLR15, and MLR16 were one-input models, which means simple linear regression models. The climate variables, namely N, Tmean, Rn, Rs, es – ea, and  $u_2$  were the inputs of the aforementioned models, respectively. Among these models, MLR1 (N input) produced the best results (adj.  $R^2 = 96.0\%$  and RMSE = 0.409 mm d<sup>-1</sup>), followed by MLR7 (Rn input) (Table 2). The Tmean input model (MLR12) exhibited inferior performance. The produced MLR equations for the two best one-input models are displayed in Table 3. The model with the poorest performance was MLR15, with  $u_2$  as the sole explanatory variable, with an adj.  $R^2$  equal to 3%. The model with es – ea as the sole input (MLR16) also showed poor performance (Table 2).

#### 4. Discussion

The ETo plays a critical role in the hydrological cycle, the climate crisis, as well as in water resource management and irrigation design. The established methods of estimation require the availability of a wide range of climate parameters, which is a serious drawback. MLR has been examined in search of a simple, affordable, and satisfactorily accurate modelling technique of ETo. Therefore, datasets of Tmean, Rn, Rs, es – ea, and u<sub>2</sub>, retrieved from sixty-two meteorological stations for the Peloponnese (Table A1) have been utilised. The altitude of the stations was also employed, since it affects ETo [65]. The months August and December of 2016–2019 were selected as typical months of summertime and wintertime, respectively, with considerable differences in climate variables between them (<http://climatlas.hnms.gr/sdi/?lang=EN> (accessed on 3 May 2022)). Furthermore, these two months were selected in methodological consistency with a previous study [36], the FAO PM estimates of which served as reference values for this study. MLR models with several input combinations of the seven available input parameters were tested. In total, sixteen models were examined, ranging from one to six explanatory variables, since models with seven inputs exhibited statistically insignificant results ( $p > 0.05$ ), and were therefore omitted. As displayed in Table 2, the results of the majority of the tested models are significant at the 99% level of confidence. Models with altitude or latitude as sole input variables were not applicable. As a general rule, the values of error and agreement improve with an ascending number of input parameters. However, the magnitude of change differentiates based on the influence of each added parameter on ETo. As anticipated, the best performance was exhibited by the model with the most (six) inputs (MLR6). However, the MLR5 model is most recommended, since the extra parameter of MLR6 (Z) contributes to the interpretation of the variance only by 0.03% (adj. R<sup>2</sup> change). The variance of the ETo observations is explained by 98.1% in both cases. For MLR5, RMSE is only 0.280 mm d<sup>-1</sup> and MAE is 0.206 mm d<sup>-1</sup>, with an agreement between the FAO PM and the MLR5 ETo values of 99.5% (Table 2). Consequently, MLR5 is a satisfactorily accurate tool for predicting ETo for August and December of 2016–2019, with a simple linear formula (Table 3). The major contribution of sunshine hours to the explanation of the data in MLR is in line with the results of Yirga for Ethiopia [61].

An interesting group of MLR models demonstrated in Table 2 are those with one sole independent variable as an input. In this case, the MLR transmits to simple linear regression. From a parsimonious perspective, the potential of only one variable being able to satisfactorily represent the ETo values would be useful in terms of (low) complexity, computational load and cost, as well as of increased applicability. The usefulness is amplified due to the rather inhomogeneous characteristics of the region, and the selected months that belong to different seasons. The only prerequisite, in this case, is that input data are available or easily retrieved. Among one-input models, MLR1 with N as the input variable exhibited the best performance, with 96% of the ETo values explained and an IoA of 99%. The RMSE/MAE and NMRSE are equal to 0.409/0.320 mm d<sup>-1</sup> and 12.1%, respectively (Table 2). According to the literature, these values are considered very good to excellent in terms of accuracy [58]. Sunshine hours is a parameter that was computed according to FAO guidelines for missing data, utilizing Julian day and station latitude [33], which might be a limitation in terms of accuracy compared to direct measurements. The methodological choice to include parameters computed based on measured parameters and the FAO procedure in ETo modelling is a common practice (e.g., in ANNs for ETo [40]). The second-best one-input model is MLR7, which is radiation-based (Rn). It explains data variability by 95.5%, with an IoA equal to 98.9%. The RMSE/MAE and NMRSE are 0.429/0.323 mm d<sup>-1</sup> and 12.7%, respectively. Residual statistical values (i.e., Cook's D, C. Leverage) were almost the same as those of MLR1, except from the D–W value, which was better (2.09), (Table 2). The latter value indicates that the residuals belong to a normal distribution.

However, the most easy-to-acquire datasets globally, by either ground-based data or remote sensing, are those of Tmean. MLR12 is a temperature-based, one-input model

(Tmean). The variability explained (91.8%) is lower than those explained by N input and Rn input models, but is the same as the corresponding of the Rs input model (MLR14). The RMSE/MAE and NRMSE are equal to 0.582/0.461 mm d<sup>-1</sup> and 17.2%. The poor performance of the Tmean input MLR model is also reported by Tabari et al. for Iran [52]. MLR14 (Rs) produced the same or slightly better values (MAE = 0.441 mm d<sup>-1</sup>) than the Tmean input model (Table 2). However, these values are almost identical to the results of Tabari et al. for the best MLR (four-input) model [52]. This accuracy is not satisfactory for applications such as precise irrigation design, but it remains a useful approach. It is noteworthy that half of the tested models (two to six inputs) yielded an RMSE below 0.35 mm d<sup>-1</sup>, three of which were even below 0.29 mm d<sup>-1</sup>, with adj. R<sup>2</sup> ≥ 97.1%. The produced linear equations for MLR5, and MLR1 and MLR7, which are, respectively, the model with the best performance, and the two best one-input models, are simple and demand low computational effort and a short time to apply (Table 3). These findings provide flexible potential choices regarding the available datasets. The worst performance was exhibited by MLR15, with u<sub>2</sub> as the sole explanatory variable. This model explains only 3% of the ETo observations. The error indices are not acceptable either (RMSE > 2.00 mm d<sup>-1</sup>, MAE = 1.953, NRMSE = 59.2%, and the SE of the predicted values was greater than 15%) (Table 2). The literature reports that near-surface wind speed is an influential parameter of ETo variability [78]. The influential role of u<sub>2</sub> in our study area was also noted in our previous work on ETo variability across the Peloponnese [36]. It was found that, mostly in August, (wind speed is generally very low in summer), in cases where increased u<sub>2</sub> values occurred, ETo was directly affected. This deduction is confirmed by the latest study on ETo across the Peloponnese, in which u<sub>2</sub> was proven to be the most influential parameter after Tmean [73]. In conclusion, it is probable that the relationship between u<sub>2</sub> and ETo is non-linear, thus the MLR model would not depict the established relationship. This inability of MLR models to portray complex relationships is anticipated due to their linear character, and has been denoted in the relevant literature [56].

## 5. Conclusions

MLR was employed to predict ETo with seven available climate parameters as inputs. Sixteen models, with all the potential input combinations, displayed statistically significant results ( $p \leq 0.05$ ). Among the tested models, MLR5 with five explanatory variables exhibited the best performance with less than the available input parameters ( $p \leq 0.001$ ). Therefore, MLR5, which constitutes a linear function of N, Tmean, Rn, es – ea, and u<sub>2</sub>, is recommended as a potential tool to predict ETo for the Peloponnese, after further investigation. Eight out of the sixteen tested models, with two to six inputs, displayed an RMSE below 0.35 mm d<sup>-1</sup>, and explained the variance of ETo at least by 97.1%. Moreover, three of these models yielded an RMSE below 0.29 mm d<sup>-1</sup>, and explained the variance by 98–98.1%.

Another noteworthy group of MLR models examined is the one-input models, which are simple linear equations. The N input model (MLR1) outperformed the rest (RMSE = 0.409 mm d<sup>-1</sup>), while it explained the variance of the ETo by 96%. The Rn model (MLR7) followed closely, with satisfactory results and data variance representation (RMSE = 0.429 mm d<sup>-1</sup>, adj. R<sup>2</sup> = 95.5%). Probably, sunshine hours and net radiation significantly affect the ETo of the Peloponnese. The Tmean input model exhibited poorer performance. On the other hand, the model with the worst performance was MLR15, with u<sub>2</sub> as the sole input. Based on previous research, which reported the influential role of u<sub>2</sub> on the ETo for the Peloponnese, it seems that MLR could not capture the complex, non-linear relationship between u<sub>2</sub> and ETo. Provided that the Peloponnese is an area with distinguished differences over short distances, and that the regimes of the examined months vary considerably, these models have the potential to provide useful tools with flexibility regarding input data, applicable for interdisciplinary purposes. It is, hence, suggested that MLR models should be tested for longer time periods and larger areas in Greece, aiming at generalisation.

**Author Contributions:** Conceptualisation, S.D. and K.G.N.; methodology, S.D. and K.G.N.; software, S.D.; validation S.D.; formal analysis, S.D.; investigation, S.D., data curation, S.D., writing—original draft preparation, S.D., writing and editing, S.D. and K.G.N.; supervision, K.G.N. All authors have read and agreed to the published version of the manuscript.

**Funding:** This research received no external funding.

**Data Availability Statement:** Data are private, available only for the review process of the present article.

**Acknowledgments:** The authors acknowledge the National Observatory of Athens (<https://meteosearch.meteo.gr> (accessed on 15 April 2022).) for ground-based data availability of sixty-two meteorological stations.

**Conflicts of Interest:** The authors declare no conflict of interest.

## Appendix A

Table A1. Meteorological stations (62) used (source: <https://meteosearch.meteo.gr> (accessed on 15 April 2022)).

ID	Station	X	Y	Elevation (m)	Municipality	ID	Station	X	Y	Elevation (m)	Municipality
<b>Meteorological Stations for the 3 Empirical Methods (ETo)</b>						<b>Meteorological Stations for the 3 Empirical Methods (ETo)</b>					
1	Kalavrita	334,349.9	4,210,128	781	Achaia	32	Oleni	282,783.4	4,177,872	61	Ilia
2	Kato Vlassia	317,683.4	4,2085,58	773	Achaia	33	Pineia	285,425.3	4,191,240	184	Ilia
3	Lappa	273,550	4,218,928	15	Achaia	34	Pirgos	273,886.9	4,171,891	22	Ilia
4	Olenia	288,845.1	4,221,654	34	Achaia	35	Vartholomio	253,773.8	4,193,127	15	Ilia
5	Panachaiko	313,491.4	4,235,800	1588	Achaia	36	Zacharo	290,302.6	4,150,806	5	Ilia
6	Panagopoula	318,709.5	4,243,842	15	Achaia	37	Amoni Sofikou	424,227.5	4,186,898	55	Korinthia
7	Panepistimio	305,972.3	4,239,289	66	Achaia	38	Derveni	362,057.1	4,221,737	5	Korinthia
8	Patra	301,697.8	4,236,694	6	Achaia	39	Isthmos	408,645.4	4,200,499	6	Korinthia
9	Rio	305,898.1	4,242,177	2	Achaia	40	Kiato	389,163.5	4,207,722	15	Korinthia
10	Romanos	313,476.1	4,235,744	228	Achaia	41	Krioneri	378,491.9	4,203,310	887	Korinthia
11	Sageika	280,638.4	4,219,575	26	Achaia	42	Loutraki	410,248.7	4,202,636	30	Korinthia
12	Argos	386,329.1	4,165,059	38	Argolida	43	Nemea	381,197.9	4,188,976	290	Korinthia
13	Didima	426,936.9	4,146,702	175	Argolida	44	Perigiali	397,303.1	4,199,344	38	Korinthia
14	Kranidi	424,615.7	4,137,411	110	Argolida	45	Trikala Korinthias	365,493.7	4,206,835	1077	Korinthia
15	Lagadia	326,139.9	4,172,057	970	Arkadia	46	Agioi Theodoroi	423,533.6	4,198,395	37	Korinthia
16	Levidi	349,386.5	4,171,330	853	Arkadia	47	Apidia	392,819.7	4,082,655	230	Lakonia
17	Lykochia	337,772.6	4,151,113	870	Arkadia	48	Asteri	386,527.1	4,076,757	8	Lakonia
18	Magouliana	334,497.7	4,171,275	1256	Arkadia	49	Geraki	384,706.6	4,094,508	330	Lakonia
19	Megalopoli	335,363	4,140,782	432	Arkadia	50	Krokees	371,576.2	4,082,640	241	Lakonia
20	Stemnitsa	330,377.8	4,157,967	1094	Arkadia	51	Molaoi	397,984.6	4,072,957	128	Lakonia

Table A1. Cont.

ID	Station	X	Y	Elevation (m)	Municipality	ID	Station	X	Y	Elevation (m)	Municipality
<b>Meteorological Stations for the 3 Empirical Methods (ETo)</b>						<b>Meteorological Stations for the 3 Empirical Methods (ETo)</b>					
21	Tripoli	359,989.3	4,152,250	650	Arkadia	52	Monemvasia	413,811.4	4,059,051	17	Lakonia
22	Vytina	339,989.8	4,170,409	1013	Arkadia	53	Sparti	360,929.9	4,101,670	204	Lakonia
23	Spetses	424,919.5	4,124,662	3	Attiki	54	Alagonia	343,840.9	4,107,863	765	Messinia
24	Taktikoupoli Troizinias	443,373.2	4,152,374	15	Attiki	55	Arfara	326,299.4	4,113,666	96	Messinia
25	Ydra	452,645.8	4,133,727	2	Attiki	56	Filiatra	285,439.9	4,115,175	65	Messinia
26	Amaliada	264,604.9	4,186,923	26	Ilia	57	Kalamata	331,127	4,098,974	5	Messinia
27	Andritsaina	314,220.3	4,152,125	731	Ilia	58	Kalamata Dytika	329,347.3	4,100,001	10	Messinia
28	Archaia Olympia	287,981.3	4,163,856	45	Ilia	59	Kardamili	347,857.7	4,074,651	13	Messinia
29	Foloi	297,082.7	4,174,732	600	Ilia	60	Kopanaki	306,288.6	4,128,741	184	Messinia
30	Katakolo	263,537.2	4,169,327	2	Ilia	61	Kyparissia	291,691	4,123,584	36	Messinia
31	Lampeia	306,840.3	4,192,041	840	Ilia	62	Pylos	294,556.8	4,087,590	5	Messinia

## References

1. Malamos, N.; Tegos, A. Advances in Evaporation and Evaporative Demand. *Hydrology* **2022**, *9*, 78. [CrossRef]
2. Shamshirband, S.; Hashemi, S.; Salimi, H.; Samadianfard, S.; Asadi, E.; Shadkani, S.; Kargar, K.; Mosavi, A.; Nabipour, N.; Chau, K.W. Predicting Standardized Streamflow index for hydrological drought using machine learning models. *Eng. Appl. Comput. Fluid Mech.* **2020**, *14*, 339–350. [CrossRef]
3. Xu, S.; Yu, Z.; Yang, C.; Ji, X.; Zhang, K. Trends in evapotranspiration and their responses to climate change and vegetation greening over the upper reaches of the Yellow River Basin. *Agric. For. Meteorol.* **2018**, *263*, 118–129. [CrossRef]
4. Dimitriadou, S.; Nikolakopoulos, K.G. Evapotranspiration Trends and Interactions in Light of the Anthropogenic Footprint and the Climate Crisis: A Review. *Hydrology* **2021**, *8*, 163. [CrossRef]
5. Djaman, K.; Balde, A.B.; Sow, A.; Muller, B.; Irmak, S.; N'Diaye, M.K.; Manneh, B.; Moukoumbi, Y.D.; Futakuchi, K.; Saito, K. Evaluation of sixteen reference evapotranspiration methods under sahelian conditions in the Senegal River Valley. *J. Hydrol. Reg. Stud.* **2015**, *3*, 139–159. [CrossRef]
6. Pereira, L.S.; Perrier, A.; Allen, R.G.; Alves, I. Evapotranspiration: Concepts and Future Trends. *J. Irrig. Drain. Eng.* **1999**, *125*, 45–51. [CrossRef]
7. Malamos, N.; Tsirogiannis, I.L.; Tegos, A.; Efstratiadis, A.; Koutsoyiannis, D. Spatial interpolation of potential evapotranspiration for precision irrigation purposes. *Eur. Water* **2017**, *59*, 303–309. Available online: [https://www.researchgate.net/publication/323030147\\_Spatial\\_interpolation\\_of\\_potential\\_evapotranspiration\\_for\\_precision\\_irrigation\\_purposes](https://www.researchgate.net/publication/323030147_Spatial_interpolation_of_potential_evapotranspiration_for_precision_irrigation_purposes) (accessed on 19 May 2022).
8. Saggi, M.K.; Jain, S. Reference evapotranspiration estimation and modelling of the Punjab Northern India using deep learning. *Comput. Electron. Agric.* **2019**, *156*, 387–398. [CrossRef]
9. Zhang, Y.; Wei, Z.; Zhang, L.; Du, J. Applicability evaluation of different algorithms for daily reference evapotranspiration model in KBE system. *Int. J. Comput. Sci. Eng.* **2019**, *18*, 361–374. [CrossRef]
10. Skarlatos, D.; Kalavrouziotis, I.K.; Montes, C.R.; Melfi, A.J.; Pereira, B.F.F. Wastewater reuse in citrus: A fuzzy logic model for optimum evapotranspiration. *Desalination Water Treat.* **2015**, *55*, 315–324. [CrossRef]
11. Ma, N.; Szilagyi, J.; Zhang, Y. Calibration-free complementary relationship estimates terrestrial evapotranspiration globally. *Water Resour. Res.* **2021**, *57*, e2021WR029691. [CrossRef]
12. Ma, N.; Szilagyi, J.; Zhang, Y.; Liu, W. Complementary-relationship-based modeling of terrestrial evapotranspiration across China during 1982–2012: Validations and spatiotemporal analyses. *J. Geophys. Res. Atmos.* **2019**, *124*, 4326–4351. [CrossRef]
13. Li, M.; Chu, R.; Islam, A.R.M.T.; Shen, S. Reference Evapotranspiration Variation Analysis and Its Approaches Evaluation of 13 Empirical Models in Sub-Humid and Humid Regions: A Case Study of the Huai River Basin, Eastern China. *Water* **2018**, *10*, 493. [CrossRef]
14. Tabari, H.; Grismer, M.E.; Trajkovic, S. Comparative analysis of 31 reference evapotranspiration methods under humid conditions. *Irrig. Sci.* **2013**, *31*, 107–117. [CrossRef]
15. Roy, D.K.; Sarkar, T.K.; Kamar, S.S.A.; Goswami, T.; Mukhtadir, M.A.; Al-Ghobari, H.M.; Alataway, A.; Dewidar, A.Z.; El-Shafei, A.A.; Mattar, M.A. Daily Prediction and Multi-Step forward Forecasting of Reference Evapotranspiration Using LSTM and Bi-LSTM Models. *Agronomy* **2022**, *12*, 594. [CrossRef]
16. Ferreira, L.B.; da Cunha, F.F. Multi-step ahead forecasting of daily reference evapotranspiration using deep learning. *Comput. Electron. Agric.* **2020**, *178*, 105728. [CrossRef]
17. Ravindran, S.M.; Bhaskaran, S.K.; Ambat, S.K. A Deep Neural Network Architecture to Model Reference Evapotranspiration Using a Single Input Meteorological Parameter. *Environ. Process.* **2021**, *8*, 1567–1599. [CrossRef]
18. Granata, F.; Di Nunno, F. Forecasting evapotranspiration in different climates using ensembles of recurrent neural networks. *Agric. Water Manag.* **2021**, *255*, 107040. [CrossRef]
19. Mosavi, A.; Edalatifar, M. A Hybrid Neuro-Fuzzy Algorithm for Prediction of Reference Evapotranspiration. In *Recent Advances in Technology Research and Education*; INTER-ACADEMIA 2018; Lecture Notes in Networks and Systems; Laukaitis, G., Ed.; Springer: Cham, Switzerland, 2019; Volume 53.
20. Andreu, A.; Kustas, W.P.; Polo, M.J.; Carrara, A.; González-Dugo, M.P. Modeling Surface Energy Fluxes over a Dehesa (Oak Savanna) Ecosystem Using a Thermal Based Two Source Energy Balance Model (TSEB) II—Integration of Remote Sensing Medium and Low Spatial Resolution Satellite Images. *Remote Sens.* **2018**, *10*, 558. [CrossRef]
21. Silva, A.M.; da Silva, R.M.; Santos, C.A.G. Automated surface energy balance algorithm for land (ASEBAL) based on automating end member pixel selection for evapotranspiration calculation in MODIS orbital images. *Int. J. Appl. Earth Obs. Geoinf.* **2019**, *79*, 1–11. [CrossRef]
22. Sidiropoulos, P.; Dalezios, N.R.; Loukas, A.; Mylopoulos, N.; Spiliotopoulos, M.; Faraslis, I.N.; Alpanakis, N.; Sakellariou, S. Quantitative Classification of Desertification Severity for Degraded Aquifer Based on Remotely Sensed Drought Assessment. *Hydrology* **2021**, *8*, 47. [CrossRef]
23. Raoufi, R.; Beighley, E. Estimating Daily Global Evapotranspiration Using Penman–Monteith Equation and Remotely Sensed Land Surface Temperature. *Remote Sens.* **2017**, *9*, 1138. [CrossRef]
24. Allen, R.G.; Tasumi, M.; Trezza, R. Satellite-based energy balance for mapping evapotranspiration with internalized calibration (METRIC)—Model. *J. Irrig. Drain. Eng.* **2007**, *133*, 380–394. [CrossRef]

25. Dimitriadou, S.; Nikolakopoulos, K.G. Remote sensing methods to estimate evapotranspiration incorporating MODIS derived data and applications over Greece: A review. In Proceedings of the SPIE 11524, Eighth International Conference on Remote Sensing and Geoinformation of the Environment (RSCy2020), Paphos, Cyprus, 26 August 2020; p. 1152405. [\[CrossRef\]](#)
26. Liu, Y.; Zhang, S.; Jiahua Zhang, J.; Tang, L.S.; Bai, Y. Assessment and Comparison of Six Machine Learning Models in Estimating Evapotranspiration over Croplands Using Remote Sensing and Meteorological Factors. *Remote Sens.* **2021**, *13*, 3838. [\[CrossRef\]](#)
27. Proias, G.; Gravalos, I.; Papageorgiou, E.; Poczeta, K.; Sakellariou-Makrantonaki, M. Forecasting Reference Evapotranspiration Using Time Lagged Recurrent Neural Network. *Wseas Trans. Environ. Dev.* **2020**, *16*, 699–707. [\[CrossRef\]](#)
28. Kitsara, G.; Papaioannou, G.; Retalis, A.; Paronis, D.; Kerkides, P. Estimation of air temperature and reference evapotranspiration using MODIS land surface temperature over Greece evapotranspiration using MODIS land surface temperature. *Int. J. Remote Sens.* **2018**, *39*, 924–948. [\[CrossRef\]](#)
29. Falalakis, G.; Gemitzi, A. A simple method for water balance estimation based on the empirical method and remotely sensed evapotranspiration estimates. *J. Hydroinform.* **2020**, *22*, 440–451. [\[CrossRef\]](#)
30. Tsouni, A.; Kontoes, C.; Koutsoyiannis, D.; Elias, P. Estimation of Actual Evapotranspiration by Remote Sensing. *Sensors* **2008**, *8*, 3586–3600. [\[CrossRef\]](#)
31. Vasiliades, L.; Spiliotopoulos, M.; Tzabiras, J.; Loukas, A.; Mylopoulos, N. Estimation of crop water requirements using remote sensing for operational water resources management. In Proceedings of the Third International Conference on Remote Sensing and Geoinformation of the Environment (RSCy2015), Paphos, Cyprus, 19 June 2015; Volume 9535. [\[CrossRef\]](#)
32. Dimitriadou, S.; Nikolakopoulos, K.G. Development of GIS models via optical programming and python scripts to implement four empirical methods of reference and actual evapotranspiration (ET<sub>o</sub>, ET<sub>a</sub>) incorporating MODIS LST inputs. In Proceedings of the SPIE 11856, Remote Sensing for Agriculture, Ecosystems, and Hydrology XXIII, 118560K, Madrid, Spain, 12 September 2021. [\[CrossRef\]](#)
33. Allen, R.; Pereira, L.; Raes, D.; Smith, M. Crop evapotranspiration—Guidelines for computing crop water requirements. In *Irrigation and Drainage, Paper No. 56*; FAO: Rome, Italy, 1998; Volume 300.
34. Pereira, L.S.; Allen, R.G.; Smith, M.; Raes, D. Crop evapotranspiration estimation with FAO 56: Past and future. *Agric. Water Manag.* **2015**, *147*, 4–20. [\[CrossRef\]](#)
35. Samani, Z. Estimating solar radiation and evapotranspiration using minimum climatological data. *J. Irrig. Drain. Eng.* **2000**, *126*, 265–267. [\[CrossRef\]](#)
36. Dimitriadou, S.; Nikolakopoulos, K.G. Reference Evapotranspiration (ET<sub>o</sub>) Methods Implemented as ArcMap Models with Remote-Sensed and Ground-Based Inputs, Examined along with MODIS ET, for Peloponnese, Greece. *ISPRS Int. J. Geo-Inf.* **2021**, *10*, 390. [\[CrossRef\]](#)
37. Djaman, K.; Rudnick, D.; Mel, V.C.; Mutibwa, D.; Diop, L.; Sall, M.; Kabenge, I.; Bodian, A.; Tabari, H.; Irmak, S. Evaluation of Valiantzas' Simplified Forms of the FAO-56 Penman-Monteith Reference Evapotranspiration Model in a Humid Climate. *J. Irrig. Drain. Eng.* **2017**, *143*, 0001191. [\[CrossRef\]](#)
38. Tegos, A.; Efstratiadis, A.; Malamos, N.; Mamassis, N.; Koutsoyiannis, D. Evaluation of a Parametric Approach for Estimating Potential Evapotranspiration across Different Climates. *Agric. Agric. Sci. Procedia* **2015**, *4*, 2–9. [\[CrossRef\]](#)
39. Valiantzas, J.D. Simplified Reference Evapotranspiration Formula Using an Empirical Impact Factor for Penman's Aerodynamic Term. *J. Irrig. Drain. Eng.* **2013**, *139*, 108–114. [\[CrossRef\]](#)
40. Zanetti, S.S.; Sousa, E.F.; Oliveira, V.P.S.; Almeida, F.T.; Bernardo, S. Estimating evapotranspiration using artificial neural network and minimum climatological data. *J. Irrig. Drain. Eng.* **2007**, *133*, 83–89. [\[CrossRef\]](#)
41. Noi, P.T.; Degener, J.; Kappas, M. Comparison of Multiple Linear Regression, Cubist Regression, and Random Forest Algorithms to Estimate Daily Air Surface Temperature from Dynamic Combinations of MODIS LST Data. *Remote Sens.* **2017**, *9*, 398. [\[CrossRef\]](#)
42. Paparrizos, S.; Matzarakis, A. Present and future responses of growing degree days for Crete Island. *Adv. Sci. Res.* **2017**, *14*, 1–5. [\[CrossRef\]](#)
43. Taki, M.; Rohani, A.; Yildizhan, H. Application of machine learning for solar radiation modeling. *Theor. Appl. Climatol.* **2021**, *143*, 1599–1613. [\[CrossRef\]](#)
44. Alvarez-Mendoza, C.; Teodoro, A.; Ramirez-Cando, L. Spatial estimation of surface ozone concentrations in Quito Ecuador with remote sensing data, air pollution measurements and meteorological variables. *Environ. Monit. Assess.* **2019**, *191*, 155. [\[CrossRef\]](#)
45. Almeida, C.R.D.; Teodoro, A.C.; Gonçalves, A. Study of the Urban Heat Island (UHI) Using Remote Sensing Data/Techniques: A Systematic Review. *Environments* **2021**, *8*, 105. [\[CrossRef\]](#)
46. Ghosh, A.; Joshi, P.K. Hyperspectral imagery for disaggregation of land surface temperature with selected regression algorithms over different land use land cover scenes. *ISPRS J. Photogramm. Remote Sens.* **2014**, *96*, 76–93. [\[CrossRef\]](#)
47. Mohammad, P.; Goswami, A. A Spatio-Temporal Assessment and Prediction of Surface Urban Heat Island Intensity Using Multiple Linear Regression Techniques Over Ahmedabad City, Gujarat. *J. Indian Soc. Remote Sens.* **2021**, *49*, 1091–1108. [\[CrossRef\]](#)
48. ASCE Task Committee on Application of Artificial Neural Networks in Hydrology. Artificial neural networks in hydrology. I: Preliminary concepts. *J. Hydrol. Eng.* **2000**, *5*, 115–123. [\[CrossRef\]](#)
49. Perugu, M.; Singam, A.J.; Kamasani, C.S.R. Multiple Linear Correlation Analysis of Daily Reference Evapotranspiration. *Water Resour. Manag.* **2013**, *27*, 1489–1500. [\[CrossRef\]](#)
50. Mallikarjuna, P.; Jyothy, S.A.; Sekhar Reddy, K.C. Daily Reference Evapotranspiration Estimation using Linear Regression and ANN Models. *J. Inst. Eng. India Ser. A* **2012**, *93*, 215–221. [\[CrossRef\]](#)

51. Khoshravesh, M.; Sefidkouhi, M.A.G.; Valipour, M. Estimation of reference evapotranspiration using multivariate fractional polynomial, Bayesian regression, and robust regression models in three arid environments. *Appl. Water Sci.* **2015**, *7*, 1911–1922. [[CrossRef](#)]
52. Tabari, H.; Kisi, O.; Ezani, A.; Talaei, P.H. SVM, ANFIS, regression and climate based models for reference evapotranspiration modeling using limited climatic data in a semi-arid highland environment. *J. Hydrol.* **2012**, *444–445*, 78–89. [[CrossRef](#)]
53. Shirsath, P.B.; Singh, A.K. A Comparative Study of Daily Pan Evaporation Estimation Using ANN, Regression and Climate Based Models. *Water Resour. Manag.* **2010**, *24*, 1571–1581. [[CrossRef](#)]
54. Sanford, W.E.; Nelms, D.L.; Selnick, J.; Pope, J.P. *Quantifying Components of the Hydrologic Cycle in Virginia Using Chemical Hydrograph Separation and Multiple Regression Analysis*; U.S. Geological Survey Scientific Investigations Report 2011-5198; USGS Science Publishing Network: Raleigh, NC, USA, 2011; p. 152.
55. Sanford, W.E.; Selnick, D.L. Estimation of Evapotranspiration across the Conterminous United States Using a Regression with Climate and Land-Cover Data. *J. Am. Water Resour. Assoc.* **2013**, *49*, 217–230. [[CrossRef](#)]
56. Niaghi, A.R.; Hassanijalilian, O.; Shiri, J. Estimation of Reference Evapotranspiration Using Spatial and Temporal Machine Learning Approaches. *Hydrology* **2021**, *8*, 25. [[CrossRef](#)]
57. Ohana-Levi, N.; Ben-Gal, A.; Munitz, S.; Netzer, Y. Grapevine crop evapotranspiration and crop coefficient forecasting using linear and non-linear multiple regression models. *Agric. Water Manag.* **2022**, *262*, 107317. [[CrossRef](#)]
58. Sharafi, S.; Ghaleni, M.M. Evaluation of multivariate linear regression for reference evapotranspiration modeling in different climates of Iran. *Theor. Appl. Climatol.* **2021**, *143*, 1409–1423. [[CrossRef](#)]
59. Soni, A.; Syed, T.H. Analysis of variations and controls of evapotranspiration over major Indian River Basins (1982–2014). *Sci. Total Environ.* **2021**, *754*, 141892. [[CrossRef](#)] [[PubMed](#)]
60. Bian, Y.; Dai, H.; Zhang, Q.; Yang, L.; Du, W. Spatial distribution of potential evapotranspiration trends in the Inner Mongolia Autonomous Region (1971–2016). *Theor. Appl. Climatol.* **2020**, *140*, 1161–1169. [[CrossRef](#)]
61. Yirga, S.A. Modelling reference evapotranspiration for Megecha catchment by multiple linear regression. *Modeling Earth Syst. Environ.* **2019**, *5*, 471–477. [[CrossRef](#)]
62. Dimitriadou, S.; Katsanou, K.; Charalabopoulos, S.; Lambrakis, N. Interpretation of the Factors Defining Groundwater Quality of the Site Subjected to the Wildfire of 2007 in Ilia Prefecture, South-Western Greece. *Geosciences* **2018**, *8*, 108. [[CrossRef](#)]
63. Copernicus Land Monitoring Service. CLC 2018. © European Union, Copernicus Land Monitoring Service 2018, European Environment Agency (EEA). Available online: <https://land.copernicus.eu/pan-european/corine-land-cover/clc2018> (accessed on 11 April 2022).
64. Kotttek, M.; Grieser, J.; Beck, C.; Rudolf, B.; Rubel, F. World Map of the Köppen-Geiger climate classification updated. *Meteorol. Z.* **2006**, *15*, 259–263. [[CrossRef](#)]
65. Wang, K.; Xu, Q.; Li, T. Does recent climate warming drive spatiotemporal shifts in functioning of high-elevation hydrological systems? *Sci. Total Environ.* **2020**, *719*, 137507. [[CrossRef](#)]
66. Rahimikhoo, A. Estimation of evapotranspiration based on only air temperature data using artificial neural networks for a subtropical climate in Iran. *Theor. Appl. Climatol.* **2010**, *101*, 83–91. [[CrossRef](#)]
67. Kuhn, M.; Johnson, K. *Applied Predictive Modeling*; Springer: New York, NY, USA, 2013. [[CrossRef](#)]
68. Gokmen, M.; Vekerdy, Z.; Verhoef, A.; Verhoef, W.; Batelaan, O.; van der Tol, C. Integration of soil moisture in SEBS for improving evapotranspiration estimation under water stress conditions. *Remote Sens. Environ.* **2012**, *121*, 261–274. [[CrossRef](#)]
69. Chen, M.; Senay, G.B.; Singh, R.K.; Verdin, J.P. Uncertainty analysis of the Operational Simplified Surface Energy Balance (SSEBop) model at multiple flux tower sites. *J. Hydrol.* **2016**, *536*, 384–399. [[CrossRef](#)]
70. Krishnashetty, P.H.; Balasangameshwara, J.; Sreeman, S.; Desai, S.; Kantharaju, A.B. Cognitive computing models for estimation of reference evapotranspiration: A review. *Cogn. Syst. Res.* **2021**, *70*, 109–116. [[CrossRef](#)]
71. Maroufpoor, S.; Bozorg-Haddad, O.; Maroufpoor, E. Reference evapotranspiration estimating based on optimal input combination and hybrid artificial intelligent model: Hybridization of artificial neural network with grey wolf optimizer algorithm. *J. Hydrol.* **2020**, *588*, 125060. [[CrossRef](#)]
72. Sattari, M.T.; Apaydin, H.; Band, S.S.; Mosavi, A.; Prasad, R. Comparative analysis of kernel-based versus ANN and deep learning methods in monthly reference evapotranspiration estimation. *Hydrol. Earth Syst. Sci.* **2021**, *25*, 603–618. [[CrossRef](#)]
73. Dimitriadou, S.; Nikolakopoulos, K.G. Artificial Neural Networks for the Prediction of the Reference Evapotranspiration of the Peloponnese Peninsula, Greece. *Water* **2022**, *14*, 2027. [[CrossRef](#)]
74. Seifi, A.; Riahi, H. Estimating daily reference evapotranspiration using hybrid gamma test-least square support vector machine, gamma test-ANN, and gamma test-ANFIS models in an arid area of Iran. *J. Water Clim. Chang.* **2020**, *11*, 217–240. [[CrossRef](#)]
75. Ferreira, L.B.; da Cunha, F.F.; de Oliveira, R.A.; Fernandes Filho, E.I. Estimation of reference evapotranspiration in Brazil with limited meteorological data using ANN and SVM—A new approach. *J. Hydrol.* **2019**, *572*, 556–570. [[CrossRef](#)]
76. Wilks, D.S. *Statistical Methods in the Atmospheric Sciences*; Academic Press: Oxford, UK; Waltham, MA, USA, 2006.
77. Willmott, C.; Matsuura, K. Advantages of the mean absolute error (MAE) over the root mean square error (RMSE) in assessing average model performance. *Clim. Res.* **2005**, *30*, 79–82. [[CrossRef](#)]
78. McVicar, T.R.; Roderick, M.L.; Donohue, R.J.; Li, L.T.; Van Niel, T.G.; Thomas, A.; Grieser, J.; Jhajharia, D.; Himri, Y.; Mahowald, N.M.; et al. Global review and synthesis of trends in observed terrestrial near-surface wind speeds: Implications for evaporation. *J. Hydrol.* **2012**, *416–417*, 182–205. [[CrossRef](#)]